Effects of Geometric Ratios on Heat Transfer in Heated Cylinders: Modelling and Simulation

O. A. Olayemi[1*], A. M. Obalalu[2], S. E. Ibitoye[3], A. Salaudeen[1], M. O. Ibiwoye[4], B. E. Anyaegbuna[3], I. K. Adegun[3]

[1]Department of Aeronautics and Astronautics, Faculty of Engineering & Technology, Kwara State University, Malete, Kwara State, Nigeria
[2]Department of Physics, Augustine University, Ilara-Epe, Lagos State, Nigeria
[3]Department of Mechanical Engineering, Faculty of Engineering & Technology, University of Ilorin, Ilorin, Nigeria
[4]Department of Mechanical Engineering, Faculty of Engineering & Technology, Kwara State University, Malete, Kwara State, Nigeria

ABSTRACT: The application of fluid and heat transfer in electronic and nuclear technology is gaining popularity, particularly in equipment's life span and risk management. However, further study is required for applications involving rectangular cylinders placed inside a square cavity. This study investigates the effects of height ratio (HR), and width ratio (WR) for Prandtl number $Pr = 0.71$ on natural convective heat transfer and the flow field around the annulus of a square domain fitted internally with a heated rectangular cylinder. The square enclosure and the inner rectangular cylinder walls were respectively maintained at cold and hot isothermal conditions. COMSOL Multiphysics (Version 5.6) software was adopted to implement the governing equations and boundary conditions. The results are presented in the form of streamlines, isothermal contours, and Nusselt number (*Nu*). The study reveals that the combined average Nu of the rectangular cylinder walls improves with HR, WR, and Rayleigh number (*Ra*). The maximum *Nu* occurred at $HR = 0.7$, and $WR = 0.7$; however, height variation at peak average Nu was 37.7% greater than width variation at peak average Nu. This study finds applications in the cooling of electronic chips and aerospace engines.

KEYWORDS: Geometric ratio, Heat transfer, Natural convection, Rectangular cylinder, Modelling and simulation

[Received Apr. 16, 2022; Revised Aug. 01, 2022; Accepted Aug. 22, 2022] Print ISSN: 0189-9546 | Online ISSN: 2437-2110

NOMENCLATURE

AR	Aspect ratio	T_c	Dimensional cold wall temperature [K]
g	Acceleration due to gravity $[m/s^2]$	T_h	Dimensional hot wall temperature [K]
H	Cylinder height $[m]$	u, v	Dimensional velocity components [ms^{-1}]
HR	Height ratio of block	U, V	Dimensionless velocity components
k	Thermal conductivity $[W/mK]$	WR	Width ratio of block
L	Dimensionless height/width of the enclosure	x, y	Dimensional Cartesian coordinates $[m]$
Nu_L	Local Nusselt number	X, Y	Dimensionless Cartesian coordinates
$\overline{Nu}$	Average Nusselt number		
p	Dimensional pressure [Nm^{-2}]		**Greek Symbols**
P	Dimensionless pressure	α	Thermal diffusivity [m^2s^{-1}]
Pr	Prandtl number	v	Kinematic Viscosity [m^2s^{-1}]
q	Heat flux $\left[W/m^2\right]$	ρ	Density [kgm^{-3}]
Ra	Rayleigh number	φ	Dimensionless temperature
T	Dimensional temperature [K]		

I. INTRODUCTION

There have been wide applications of natural convection in numerous fields such as cooling of electronic systems and nuclear devices, thermal insulation, solar devices, etc. The growing relevance of natural convection in the Engineering fields has necessitated the investigations of thermal and fluid flow behaviours in cavities of diverse shapes using both Newtonian and non-Newtonian fluids (Aithal, 2016; Pandey et al., 2019; Olayemi et al. 2022a). The first accurate computational solution of equations that describe 2-D natural convection in a square enclosure subjected to various thermal boundary conditions was done by De Vahl Davis (1983). In

*Corresponding author: olalekan.olayemi@kwasu.edu.ng

doi: http://dx.doi.org/10.4314/njtd.v19i4.1

recent times, because many similar works had been done prior to 2019, many researchers have also carried out multiple studies with similar cavities using different solution methods (Obalalu, 2021; Olayemi et al., 2021a; Olayemi et al., 2021b).

Natural convection heat transfer in a cavity having different shapes of heat sources like a triangle (Altaee and Mahdi, 2017), circular (Aithal, 2016; Pandey et al., 2019), and elliptical (Sheikholeslami et al., 2017) cylinders were carried out in 2-D to examine the influence of Rayleigh number and cavity ratio on thermal and flow distributions. Adegun et al. (2020), and Olayemi et al. (2022b) investigated the impact of cylinder orientation and size on the impact of heat transfer augmentation. Both studies reported heat transfer enhancement with increasing size of the cylinder and that the cylinder transferred maximum heat when in a horizontal position.

Buoyancy flow in a tilted cavity filled with air was investigated using the Lattice Boltzmann method for the simulation (Zhang and Che, 2014; Hssikou, 2019; Rehhali et al., 2019). It was concluded that the Lattice Boltzmann method yielded better solutions to several practical problems than most numerical methods. Some researchers also worked on inclined cavities filled with non-Newtonian nanofluids having porous medium (Raizah et al., 2018) and micropolar-nanofluid under magnetic field influence (Karagiannakis et al., 2020).

Saeid (2017) conducted a numerical analysis of natural convection in a domain equipped with discrete heating at the base of the enclosure. It was noted that increasing the height of the heating element was capable of augmenting heat transfer. Pratap Singh et al. (2020) investigated two-dimensional buoyancy flow in an asymmetric-arc-shaped cavity with a heated base and an insulated top wall. Ahmed et al. (2018) reported their findings on the convective flow in arc and circular cavities occupied by Cu-water nanofluid. The circular cavity exhibits better heat transfer results than arc cavities. Hsu et al. (2016) and Ilyas et al. (2017) experimentally worked on convective flow in an enclosure, while the convection process in a square containing freezing water was considered numerically by Ezan and Kalfa (2016). The findings revealed that wall thickness growth discourages local heat transfer within the cavity. Hussain and Ahmed (2018) used Buongiorno's nanofluid in a porous cavity to analyze the influence of Rayleigh number (104 - 107), Darcy number (10-2 -10-6), Lewis number (0.1-1), buoyancy ratio number (0.1 – 1) and Brownian motion parameter (0.1 -1) on heat transfer and fluid flow.

Ma et al. (2019) examined the numerically buoyancy-driven flow of a U-shaped cavity filled with nanofluid. The effects of Hartman number, cavity aspect ratio, nanoparticles' presence on heat enhancement, and fluid flow characteristics were investigated. They used the Lattice Boltzmann method (LBM) to analyze. Reports showed that an increase in Rayleigh number significantly impacts the argumentation of heat transfer at larger values of cavity ratio.

The present study analyzes the effect of Rayleigh number (10^2 ≤ Ra ≤ 10^6), width ratio (WR) and height ratio (HR) on fluid flow and heat transfer augmentation around a rectangular cylinder fitted in a square enclosure. The uniqueness of the present study is that there is a paucity of information in the literature on fluid flow and heat transfer around a heated rectangular cylinder placed inside a square cavity; therefore, the present work attempts to close this gap. The current study finds practical applications in electronic cooling chips, nuclear technology, the food processing industry, and finally, the results could also guide experimentalists.

II. METHODOLOGY

A. *Description of the Physical Model*

Figure 1 depicts the model, the coordinate system applied in the current analysis, and the mesh generated. The model comprises a square enclosure with dimension $L \times L$, and a rectangular cylinder fitted concentrically into the enclosure. H is cylinder's height, and W , its width. The configuration has a width ratio, $WR = \frac{W}{L}$ and a height ratio of $HR = \frac{H}{L}$. The annulus of the configuration is filled with air. The fluid flow and heat transfer in the domain are assumed to be 2-dimensional, and laminar has a natural convective flow mechanism. The cold solid boundaries of the enclosure are subjected to a dimensionless temperature, $\varphi_c = 0$ while the cylinder is fixed to a higher temperature ($\varphi_h = 1$). Fluid properties are invariant except for density, whose variation is captured by the Boussinesq approximation (Olayemi *et al*., 2021c). The walls of the enclosure have zero fixed velocity.

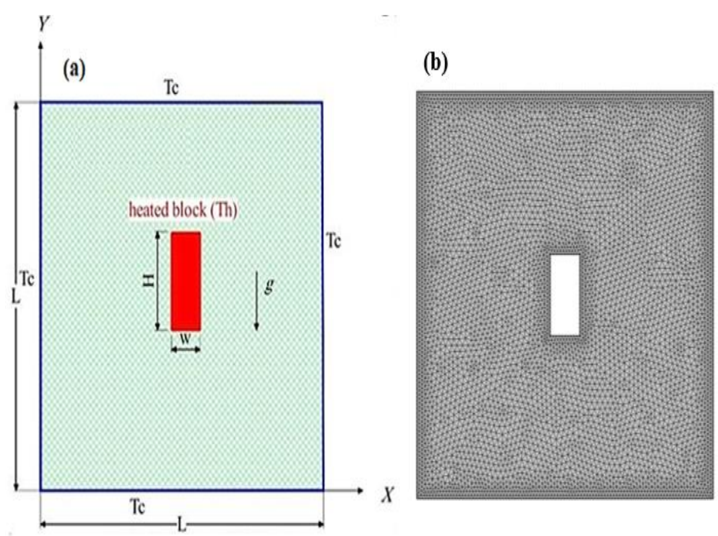

Figure 1: Schematic of (a) the problem domain and (b) mesh.

B. *Governing Equations*

The dimensional fluid motion equations for steady-state case, which are respectively continuity equation, x, and y-momentum equations, and energy equation, are expressed as (Kaminski and Prakash, 1986):

$$\frac{\partial u}{\partial x} + \frac{\partial v}{\partial y} = 0 \tag{1}$$

$$\rho\left(u\frac{\partial u}{\partial x} + v\frac{\partial u}{\partial y}\right) = -\frac{\partial p}{\partial x} + \mu\left[\frac{\partial^2 u}{\partial x^2} + \frac{\partial^2 u}{\partial y^2}\right] \tag{2}$$

$$\rho\left(u\frac{\partial v}{\partial x}+v\frac{\partial v}{\partial y}\right)=-\frac{\partial p}{\partial y}+\mu\left[\frac{\partial^2 v}{\partial x^2}+\frac{\partial^2 v}{\partial y^2}\right]+\rho g\beta(T_h-T_c) \quad (3)$$

The energy equation is expressed as:

$$u\frac{\partial T}{\partial x}+v\frac{\partial T}{\partial y}=\alpha\left(\frac{\partial^2 T}{\partial x^2}+\frac{\partial^2 T}{\partial y^2}\right) \quad (4)$$

The normalized equations governing the physics of flow are the continuity, momentum (X and Y directions), and energy equations, which are given respectively by Eqns. 5-8 as adopted by Olayemi et al., (2022c) and Olayemi et al., (2022d):

$$\frac{\partial U}{\partial X}+\frac{\partial V}{\partial Y}=0 \quad (5)$$

$$U\frac{\partial U}{\partial X}+V\frac{\partial U}{\partial Y}=-\frac{\partial P}{\partial X}+Pr\left[\frac{\partial^2 U}{\partial X^2}+\frac{\partial^2 U}{\partial Y^2}\right] \quad (6)$$

$$U\frac{\partial V}{\partial X}+V\frac{\partial V}{\partial Y}=-\frac{\partial P}{\partial Y}+Pr\left[\frac{\partial^2 V}{\partial X^2}+\frac{\partial^2 V}{\partial Y^2}\right]+RaPr\varphi \quad (7)$$

$$U\frac{\partial \varphi}{\partial X}+V\frac{\partial \varphi}{\partial Y}=\frac{\partial^2 \varphi}{\partial X^2}+\frac{\partial^2 \varphi}{\partial Y^2} \quad (8)$$

The transformation parameters used in converting the dimensional equations to their equivalent dimensionless forms are defined in Eqn. (9):

$$X=\frac{x}{L},\quad Y=\frac{y}{L},\ U=\frac{uL}{\alpha},\ V=\frac{vL}{\alpha},\ \varphi=\frac{T-T_c}{T_h-T_c},\ P=\frac{pL^2}{\rho\alpha^2},\quad Pr=\frac{v}{\alpha} \quad (9)$$

C. Boundary Conditions Imposed

On all the walls, $U=V=0$, and all the solid boundaries of the square domain are fixed at a cold non-varying dimensionless temperature of $\varphi_c=0$, while the walls of the rectangular cylinder are set to an isothermal temperature of $\varphi_h=1$.

D. *Solution Techniques*

The solution to the present study was approached with the aid of the finite element method. The Boolean operation created the annulus between the square enclosure and the enclosed cylinder. The working fluid (i.e., air) was then applied to the model. The prevailing boundary conditions were imposed on the enclosure and the cylinder walls. The domain of interest was discretized by using the extremely fine grid size option to ensure enhanced field resolution, and after that, the mesh of the domain was generated using the free triangular mesh option. The normalized equations (5 - 8) governing the flow physics and the boundary conditions applied along with the associated boundary conditions were implemented using COMSOL Multiphysics 5.6 software.

The mesh independence test was performed by using various default COMSOL Multiphysics mesh sizes corresponding to G1-G6. The relative errors of the meshes were computed, and the mesh size G5 yielded the least relative percentage error; therefore, the mesh size G5 was adopted for the entire simulation. Parametric sweep was used to investigate the impacts of height ratio (0.1 ≤ HR ≤ 0.7) and width ratio (0.1 ≤ WR ≤ 0.7) for Prandtl number of 0.71 on convective heat transfer and fluid flow in the domain investigated.

E. Determination of Nusselt Number

Nusselt number is a parameter that is used in quantifying heat transfer rate. It is expressed as the ratio of the heat convected to heat conducted via a given fluid thickness. Local Nusselt number (〖Nu〗 L) and mean Nusselt number ((Nu)̅) on the solid boundaries are given by Eqns 10 and 11, respectively (Olayemi et al., 2022c &2022d):

$$Nu_L=\frac{qL}{T_h-T_c} \quad (10)$$

$$\overline{Nu}=\frac{1}{L}\int_0^L-\frac{\partial\varphi}{\partial X}dY \quad (11)$$

III. RESULTS AND DISCUSSION

A. Validation of Results

The mesh independence study was conducted by computing the average Nusselt number on the enclosure walls, and the results are displayed in Table 1.

Table 1 shows that the average Nusselt number of the enclosure walls is independent of the mesh size for the mesh G5. Furthermore, the validation of the code used for the current investigation was done by comparing the data obtained from the geometry investigated in the absence of the inner rectangular cylinder with those in Table 2 as obtained by De Vahl Davis (1983) and Zhang and Che (2014) under the same heating conditions, and the comparison confirms an excellent agreement.

Table 1: Grid independence test of the ($\overline{Nu}$) on the enclosure walls for Ra=10^6 and AR=0.7

Size of mesh	Mesh elements	Average Nusselt number	% Error
G1	4692	5.8713	–
G2	5596	5.8705	0.013
G3	5638	5.8696	0.015
G4	6956	5.8690	0.010
G5	10536	5.8694	0.007
G6	25762	5.8765	0.121

Table 2: Comparison of optimum *Nu*, velocity components, and their corresponding coordinates.

Ra		Nu_{max}	y_{Nu}	V_{max}	x_{max}	U_{max}	y_{max}
10^3	Present work	1.5062	0.9117	3.6998	0.1820	3.6461	0.8056
	De Vahl Davis (1983)	Nil	Nil	3.6970	0.1780	3.6490	0.8130
	Zhang and Che (2014)	1.5017	0.9141	3.7024	0.1797	3.6492	0.8125
10^4	Present work	3.5302	0.8600	19.6420	0.1238	16.1992	0.8218
	De Vahl Davis (1983)	3.5309	0.8531	19.6295	0.1193	16.1802	0.8265
	Zhang and Che (2014)	3.5351	0.8564	19.6064	0.1198	16.1708	0.8229
10^5	Present work	7.7100	0.9200	68.6983	0.0648	35.5077	0.8542
	De Vahl Davis (1983)	7.7201	0.9180	68.6396	0.0657	34.7399	0.8558
	Zhang and Che (2014)	7.7472	0.9219	68.5190	0.0664	34.7110	0.8555
10^6	Present work	17.4700	0.9600	218.5459	0.0400	64.9056	0.8542
	De Vahl Davis (1983)	17.5360	0.9608	220.4610	0.0390	64.8367	0.8505
	Zhang and Che (2014)	17.6140	0.9648	219.3340	0.0391	64.8687	0.8516

B. *Effects of Width Ratio and Height Ratio on Velocity and Isothermal Contours*

The plots in Figures 2(a) and (b) depict the velocity streamlines while Figures 2(c) and (d) represent the isothermal lines for different height ratio**s** ($0.1 \leq HR \leq 0.7$) and width ratios ($0.1 \leq WR \leq 0.7$) when $Ra = 10^6$. When $WR = HR = 0.1$, the streamlines patterns both have two secondary isolated vortices close to the base of the cavity moving in opposite directions due to the presence of the inner block. As *HR* rises in value, there appear secondary circulations on top of the inner cylinder (see Figure 2(a)), which move upward as *HR* value increases.

Also, as *HR* increases in value, the surface area available for heat transfer increases. Ultimately, this leads to improved heat transfer augmentation, which is evident in forming the plumes above the inner rectangular cylinder. The trend of heat transfer augmentation for *WR* variation is similar to that of *HR* variation. Furthermore, for $WR > 0.1$ and $HR > 0.1$, the isolated vortices close to the cavity base when $WR = HR = 0.1$ disappear, and the disappearance of these secondary vortices could be due to higher buoyancy force at the top region of the inner cylinder relative to its bottom region. Around the base of the rectangular cylinder in Figure 2(d), the plots show a progressive growth in the heat transfer rate compared to that around the cylinder base in Figure 2(c); this is evidently due to the larger surface area available for heat transfer at the base of the inner rectangular cylinder in Figure 2(d). The trends reported above for the isotherms and streamlines for width ratio variation are consistent with the streamlines and isotherms reported by Olayemi *et al.* (2021), while the impact of *HR* variation for *HR* =0.5 and 0.7 is similar to the observations made by Ragui *et al.* (2013) where two secondary circulations were located close to the top horizontal wall of the enclosure.

C. *Effects of WR and HR on Local Nusselt Number*

In Figures 3(a) and (b), the plots show the local Nusselt number variation along the left wall of the square domain for various HR and WR at $Ra = 10^6$. Compared with $HR = 0.1$, the $WR = 0.1$ exhibits a higher heat transfer enhancement. However, for $0.1 < HR \leq 0.7$, the heat transfer rate along the left wall of the square domain is higher than that presented in the range $0.1 < WR \leq 0.7$. The peak value of local Nusselt number in Figure 3(a) is 9.4, which occurred when $HR = 0.7$, whereas the maximum value of the local Nusselt number in the plots of Figure 3(b) is 6.7, and it occurred when $WR = 0.5$. It is pertinent to point out that the occurrence of the optimum Nusselt number around

the vicinity of the top wall of the enclosure is due to the formation of vortices around the enclosure top wall; this same effect is also revealed in the formation of plumes around the top of the enclosure wall (See Figure 2).

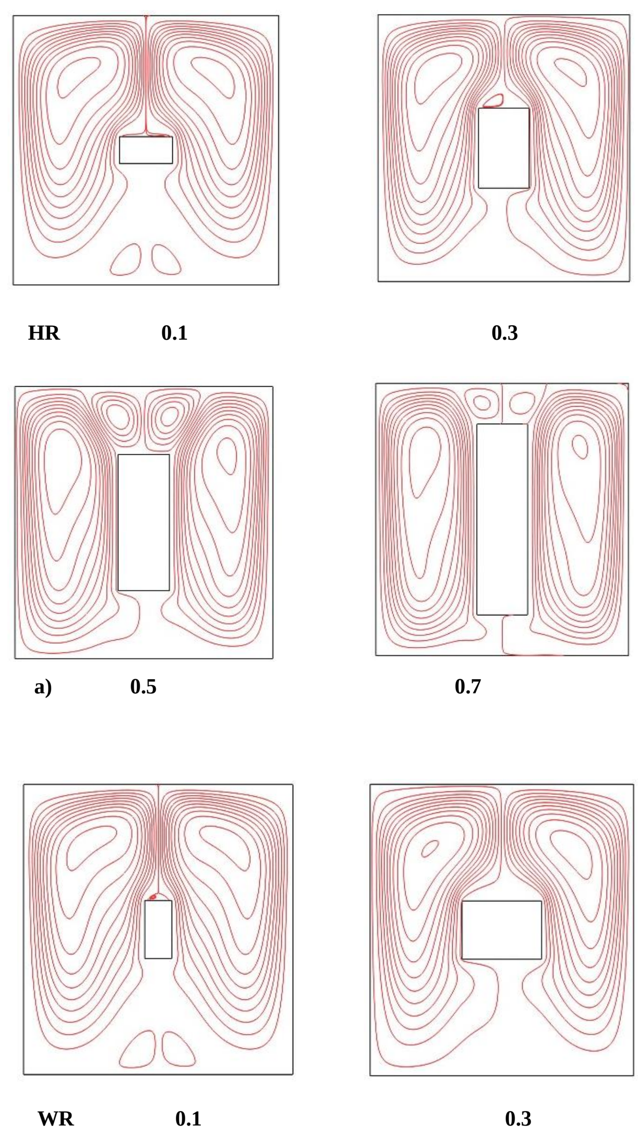

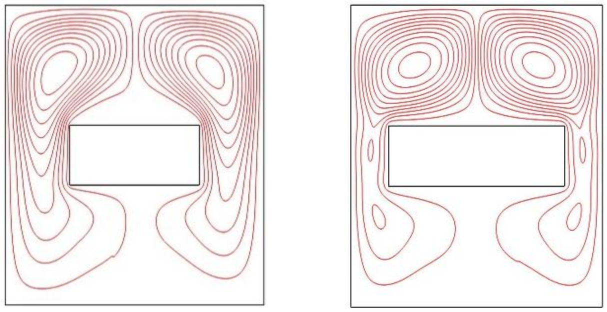

b) **0.5** **0.7**

Along the top horizontal wall of the enclosure, the local Nusselt number against wall-length plots is shown in Figure 4(a) and (b) for both HR and WR at $Ra = 10^6$. For $WR \leq 0.7$, the plots in Figure 4 show that the values of local Nusselt number improve from the base of the wall and then peak at the mid-length of the wall and reduce along the wall length. In Figure 4(a), for the height of $0.1 \leq HR \leq 0.3$, the heat transfer patterns are similar to that of Figure 4(b). However, for $HR > 0.3$, the local Nusselt number distribution assumes a sinusoidal pattern.

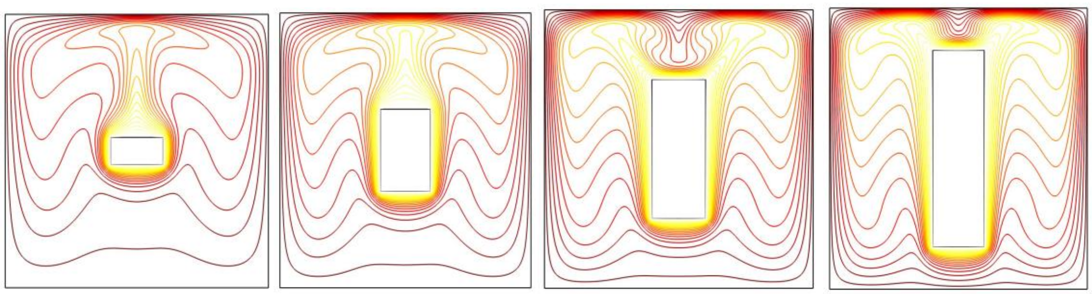

c)

HR 0.1 0.3 0.5 0.7

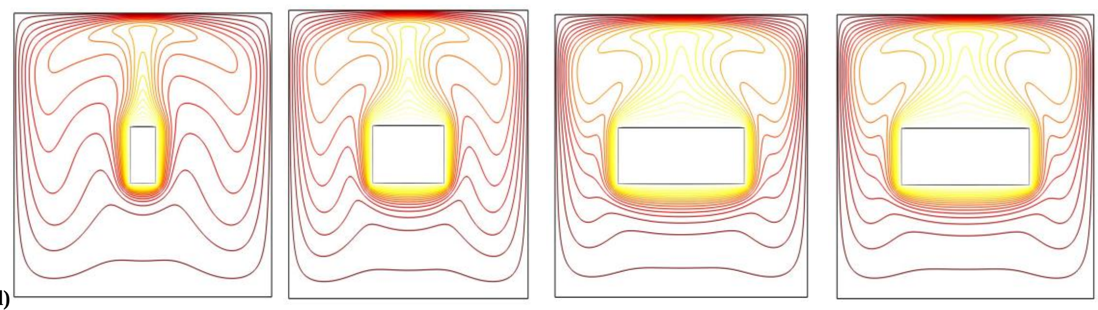

d)

WR 0.1 0.3 0.5 0.7

Figure 2: Velocity streamline ((a) and (b)) and isothermal ((c) and (d)) plots at $Ra = 10^6$ for various HR and WR.

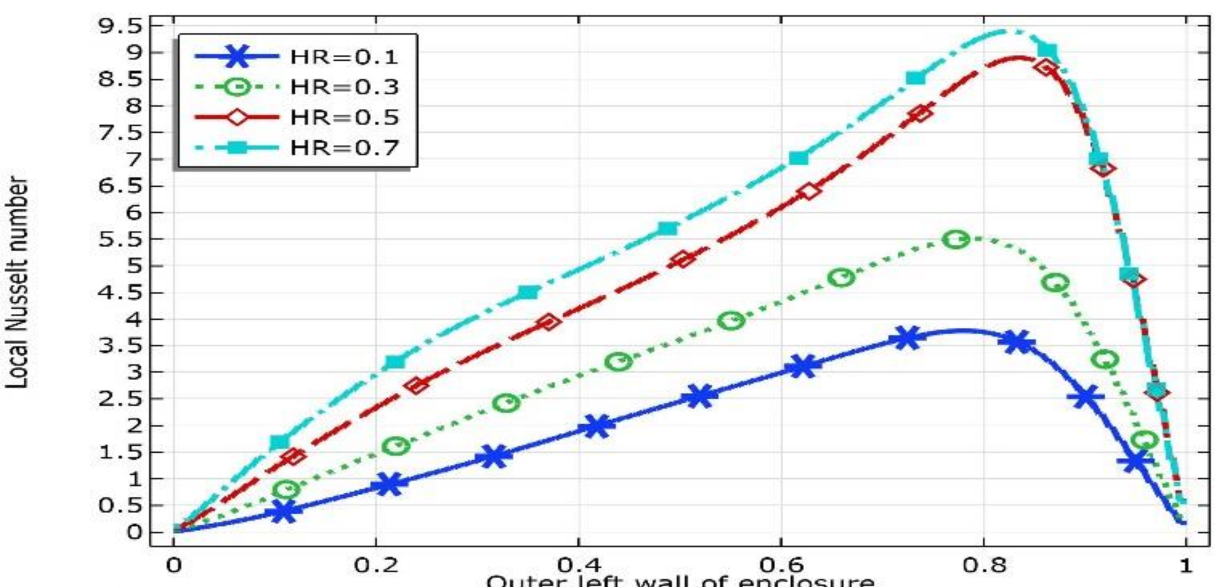

a)

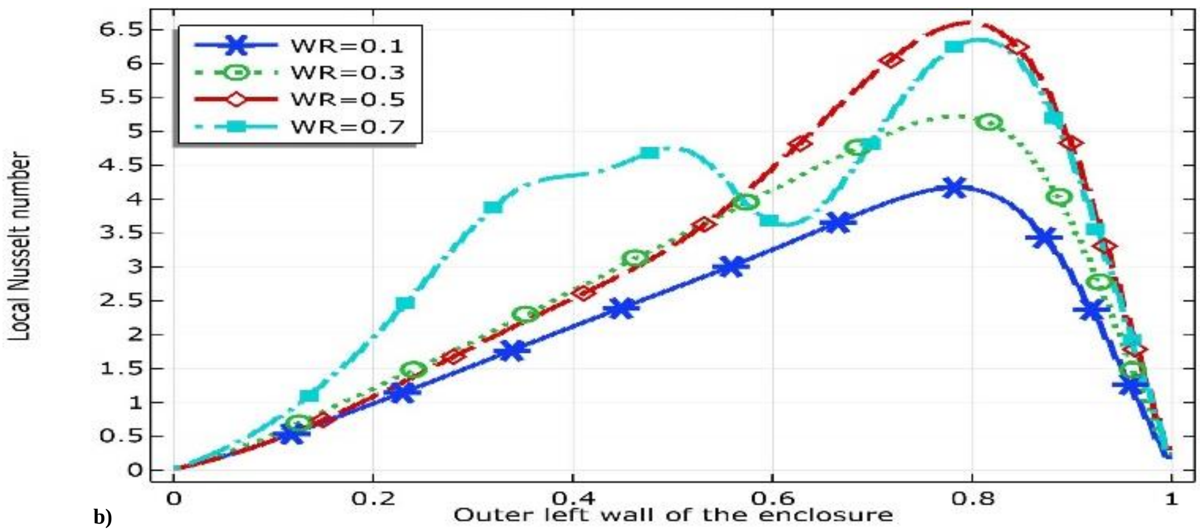

b)

Figure 3: Local Nusselt number of the square cavity left wall at $Ra = 10^6$, for various a) HR and b) WR.

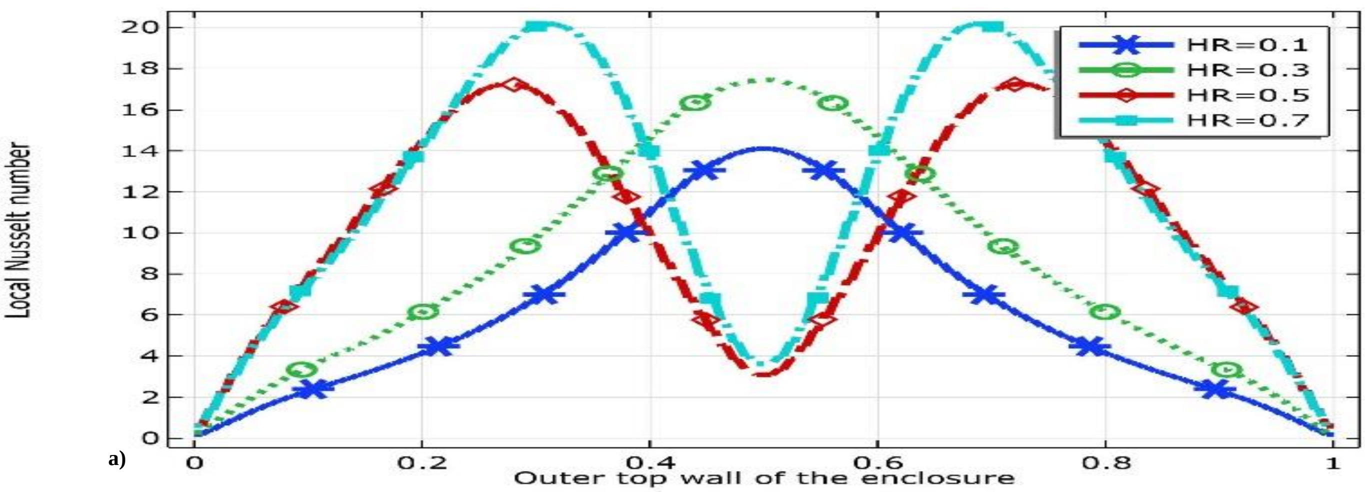

a)

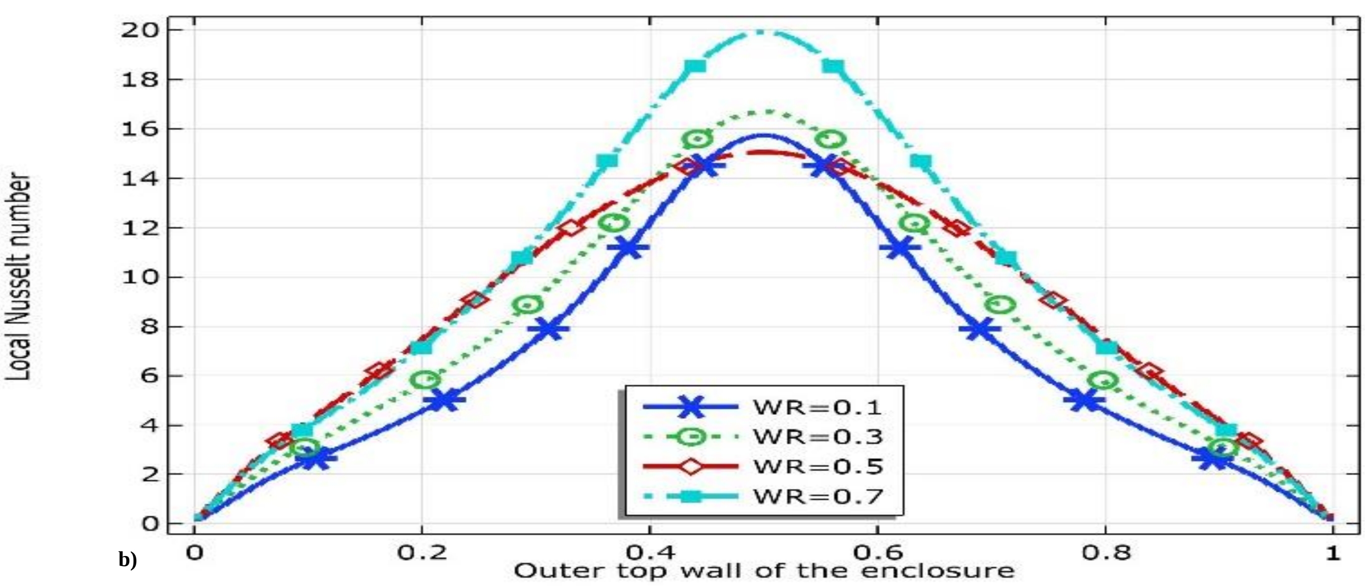

b)

Figure 4: Local Nusselt number of the square cavity top wall at $Ra = 10^6$ for various a) HR and b) WR.

Furthermore, the highest local Nusselt number (20) in Figure 4(b) occurred when $WR = 0.7$ at 50% of the wall length from its base; but in Figure 4a, the peak value of local Nusselt number (21) occurred when $HR = 0.7$, at 30% and 70% of the wall lengths from its base.

Figures 5(a) and (b) depict the local Nusselt number versus arc length (square cavity bottom wall) for various height ratios HR and width ratios WR at $Ra = 10^6$.

The rate of heat transfer for $WR = 0.1$ is 12.9% more than the rate of heat transfer for $HR = 0.1$. The rate of heat transferred for HR in the range $0.1 < HR \leq 0.7$ is greater than that transferred for width ratio in the $0.1 < WR \leq 0.7$. The highest value of the local Nusselt number (2.5) occurred when $HR = 0.7$, at the mid-point of the wall length and is 81.6% greater than the peak value of the local Nusselt number (0.46) on the same wall when $WR = 0.7$.

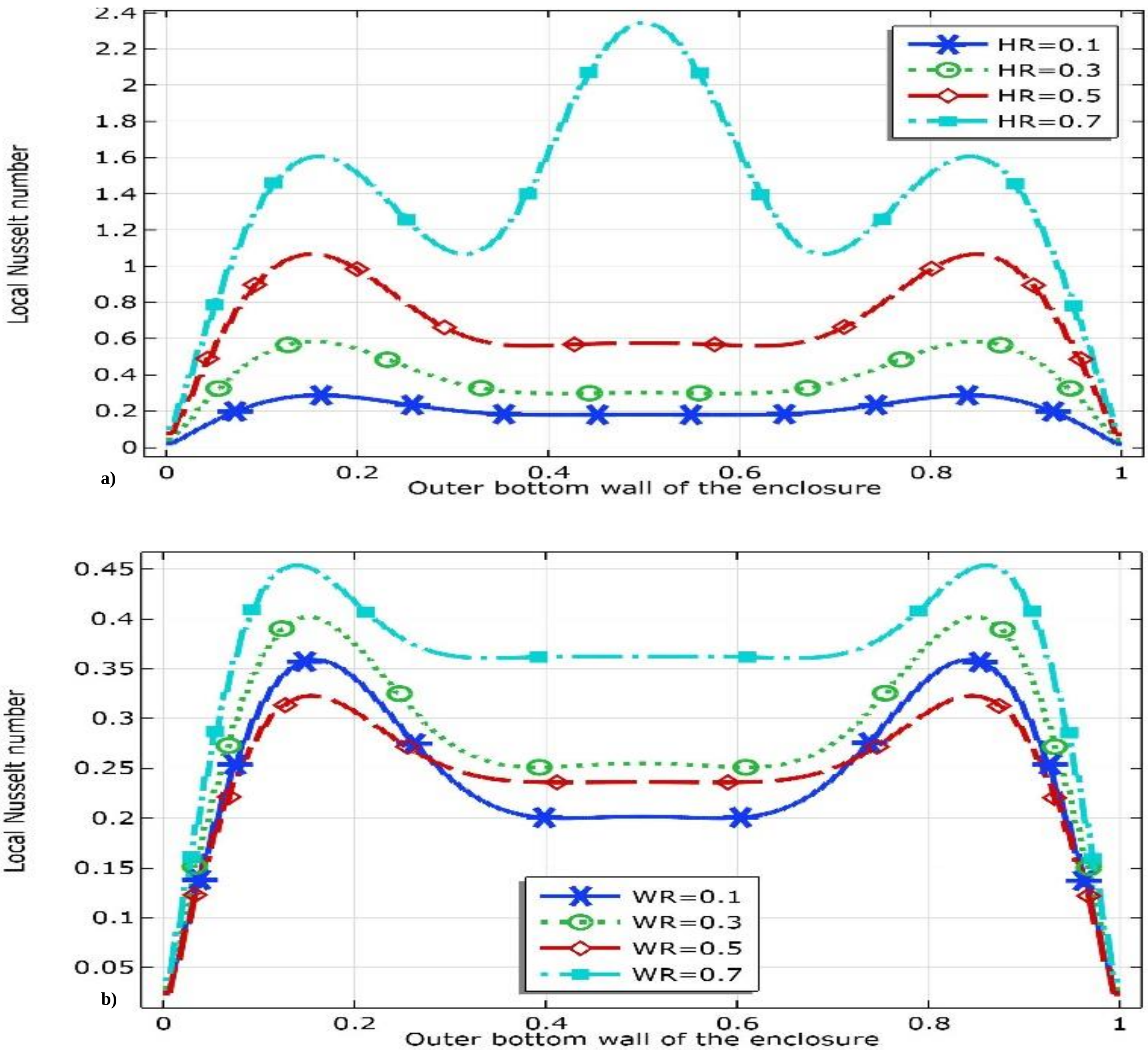

Figure 5: Local Nusselt number of the square cavity bottom wall at $Ra = 10^6$, for various a) HR and b) WR.

D. *Effects of Width Ratio, Height Ratio and Rayleigh Number (Ra) on Average Nusselt Number*

Figure 6 is the average Nusselt number for each of the walls of the cylinder for various HR and WR at $Ra = 10^6$. Figure 6(a) revealed that the heat transfer patterns on the left and right walls are the same and the average Nusselt number values are favoured by increasing HR. In Figure 6(b), the left and right walls transfer heat simultaneously, but the Nusselt number declines with increasing WR. Similarly, in Figure 6(a), the average Nusselt number of the bottom wall decreases with increasing HR, while in Figure 6(b), the WR increment augments heat transfer. Furthermore, for the top wall, in the range of HR ($0.3 \leq HR \leq 0.5$), there occurred heat transfer rate enhancement with increasing HR as revealed by Figure 6(a), this pattern is featured in the entire length of the wall for all the width ratios ($0.1 \leq WR \leq 0.7$) considered. Outside the range of height ratios of $0.3 \leq HR \leq 0.5$, wall-length increment resulted in a decline in heat transport.

The plots in Figure 7 depicts the response of the average Nusselt number of the rectangular cylinder to the variation of the Rayleigh number for various height and width ratios. The plots indicate that the average Nusselt number of the cylinder gets enhanced as the Rayleigh number rises. Additionally, HR and WR increments resulted in heat transfer augmentation, with the highest heat transfer rate occurring for each of the plots at $Ra = 10^6$ when $WR = HR = 0.7$. The peak value of the average Nusselt number on the cylinder wall occurred when $HR = 0.7$, and was found to be 37.7% higher than the average Nusselt number when $WR = 0.7$.

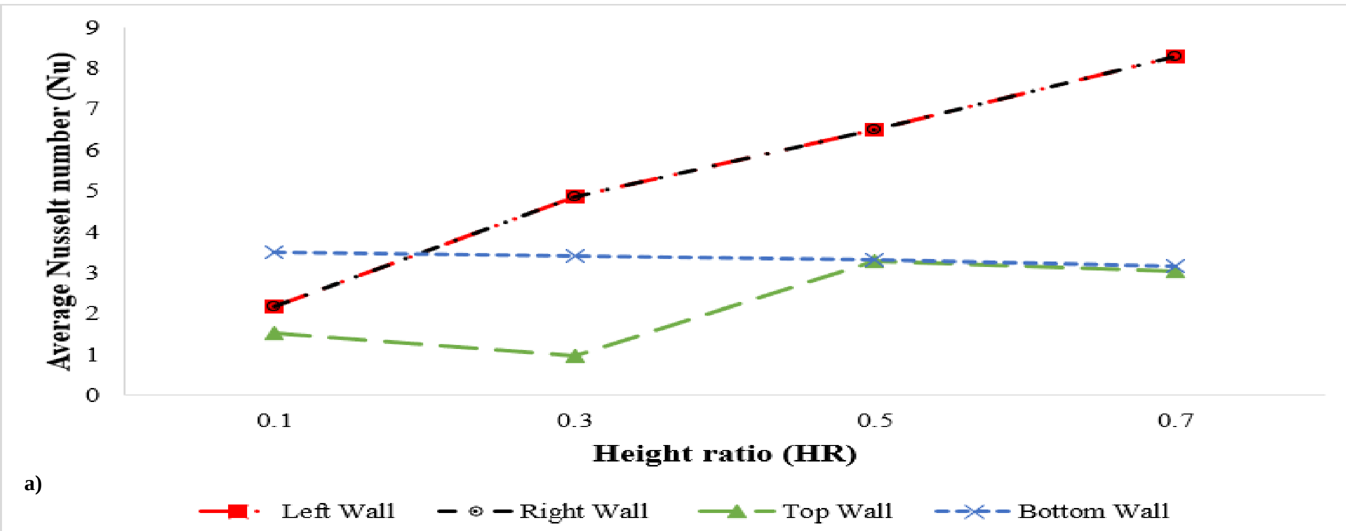

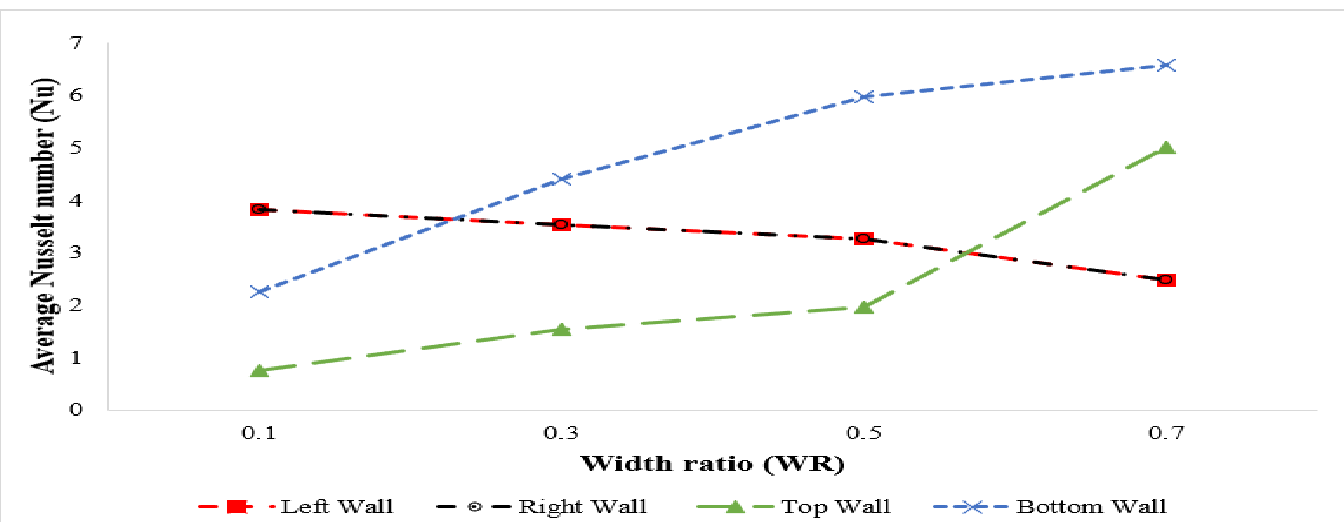

b)

Figure 6: A plot of the average Nusselt number against (a) HR and (b) WR for all the rectangular walls at $Ra = 10^6$.

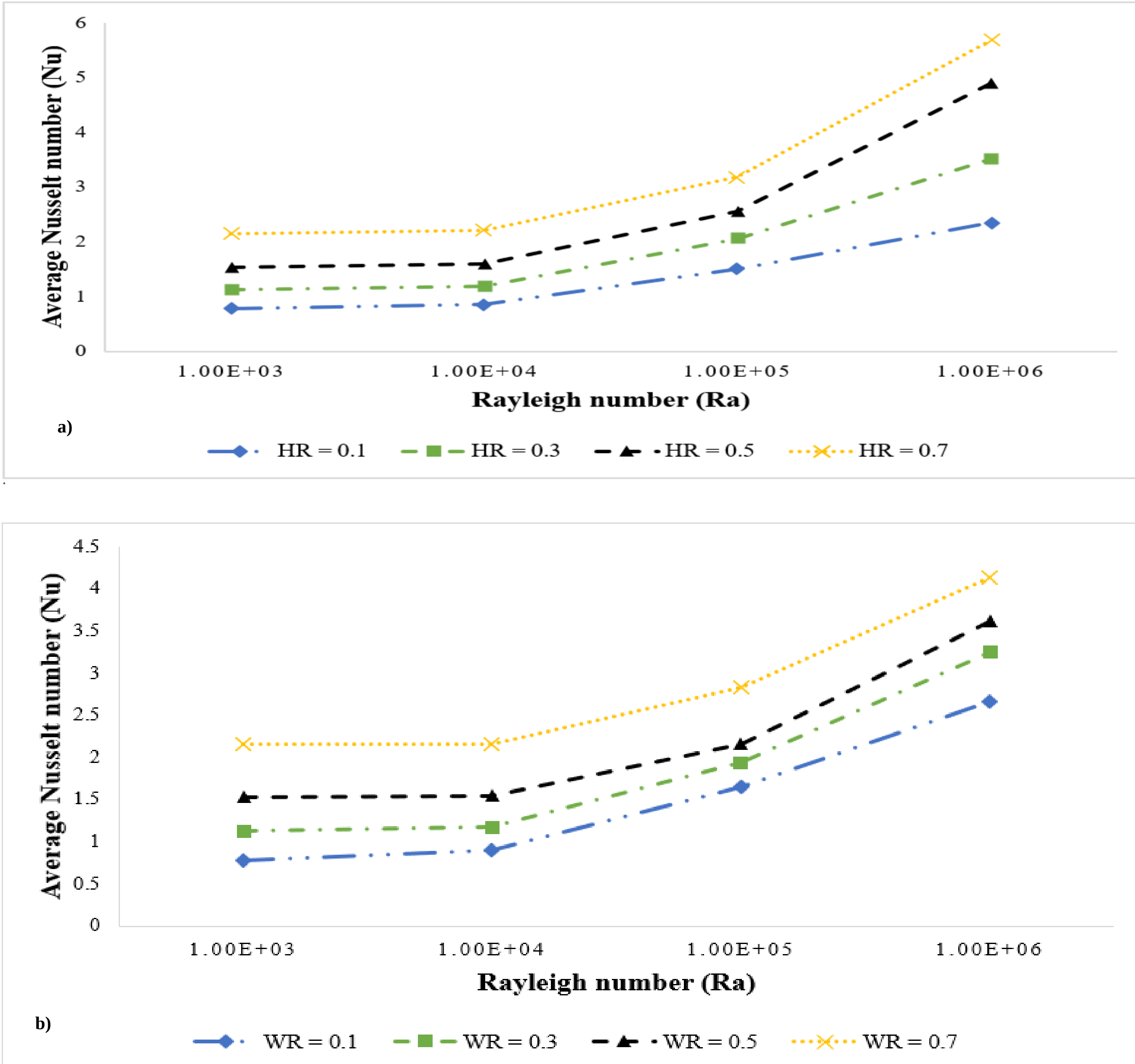

Figure 7: The plot of the average Nusselt number against Rayleigh number for (a) height ratio and (b) width ratio of the rectangular cylinder.

IV. CONCLUSION

A comprehensive numerical study of the effects of geometric ratios and Rayleigh number on fluid flow and heat transfer in a heated cylinder was studied, and the following conclusions can be drawn:

i. In the range of $0.1 < HR \leq 0.7$, the left wall of the square enclosure augmented heat better than in the range $0.1 < WR \leq 0.7$. But $WR = 0.1$ presented a better heat transfer augmentation than when $HR = 0.1$;

ii. The peak value of heat transfer on the top wall of the enclosure for $HR = 0.7$ is 10% greater than the peak value of heat transfer on the same wall when $WR = 0.7$;

iii. The highest values of the local Nusselt number of the square enclosure bottom wall are 2.5 and 0.46 when $HR = 0.7$, and $WR = 0.7$, respectively.

For the top wall of the cylinder, at a HR of $0.3 \leq HR \leq 0.5$ and WR of $0.1 \leq WR \leq 0.7$, the average Nusselt number increases with Rayleigh number, height and width ratios except for HR ranges of $0.1 < HR < 0.3$, and $0.5 < HR \leq 0.7$. Additionally, the peak value of the average Nusselt number on the cylinder wall occurred when $HR = 0.7$ and $WR = 0.7$.

AUTHOR CONTRIBUTIONS

Olayemi, O. A. conducted the simulation while **A. M. Obalalu, S. E. Ibitoye, A. Salaudeen, M. O. Ibiwoye** and **B. E. Anyaegbuna** reported the results generated while **Adegun, I. K.** and **Olayemi O. A.** reviewed the manuscript.

REFERENCES

Adegun, I. K.; S. E. Ibitoye and A. Bala. (2020). Effect of selected geometric parameters on natural convection in the concentric square annulus. Australian Journal of Mechanical Engineering, 1-12. https://doi.org/10.2514/1.T4873.

Ahmed, K. F. U.; R. Nasrin and M. Elias. (2018). Natural convective flow in circular and arc cavities filled with water-Cu nanofluid: a comparative study. Journal Naval. Architecture and Marine Engineering, 15(1): 37-52. https://doi.org/10.3329/jname.v15i1.33549.

Aithal, S. M. (2016). Turbulent natural convection in a square cavity with a circular cylinder. Journal of Thermophysics and Heat Transfer, 30(4): 843-853.

Altaee, A. H.; F. H. Ali and Q. A. Mahdi. (2017). Natural convection inside square enclosure containing equilateral triangle with different orientations. Journal of University of Babylon, 25(4): 1194-1205.

de Vahl Davis, G. (1983). Natural convection of air in a square cavity: a bench mark numerical solution. International Journal for numerical methods in fluids, 3(3): 249-264. https://doi.org/10.1002/fld.1650030305

Ezan, M. A., and Kalfa, M. (2016). Numerical investigation of transient natural convection heat transfer of freezing water in a square cavity. International Journal of Heat and Fluid Flow, 61: 438-448. https://doi:10.1016/j.ijheatfluidflow.2016.06.004.

Hssikou, M.; Y. Elguennouni; J. Baliti and M. Alaoui. (2019). Lattice Boltzmann method for natural convection in a square cavity with a heated chip. In 2019 International Conference on Intelligent Systems and Advanced Computing Sciences (ISACS) (pp. 1-7). IEEE.

Hsu, H. J.; Y. H. Huang and Y. H. Liu. (2016). Natural convection in an oscillating cylindrical enclosure with pin fins. International Journal of Heat and Mass Transfer, 93: 720-728. https://doi 10.1016/j.ijheatmasstransfer.2015.10.057.

Hussain, S., and Ahmed, S. E. (2019). Steady natural convection in open cavities filled with a porous medium utilizing Buongiorno's nanofluid model. International Journal of Mechanical Sciences, 157: 692-702. https://doi:10.1016/j.ijmecsci.2018.10.071.

Ilyas, S. U.; R. Pendyala and M. Narahari. (2017). An experimental study on the natural convection heat transfer in rectangular enclosure using functionalized alumina-thermal oil-based nanofluids. Applied Thermal Engineering, 127:765-775. https://doi.org/10.1016/j.applthermaleng.2017.08.088

Kaminski, D. A., Prakash, C. (1986). Conjugate natural convection in a square enclosure: effect of conduction in one of the vertical walls. International Journal of Heat and Mass Transfer, 29(12): 1979-1988.

Karagiannakis, N. P.; G. C. Bourantas; E. D. Skouras; V. C. Loukopoulos; K. Miller and V. N. Burganos. (2020). Modeling the natural convection flow in a square porous enclosure filled with a micropolar nanofluid under magnetohydrodynamic conditions. Applied Sciences, 10(5): 1633.

Ma, Y.; R. Mohebbi; M. M. Rashidi; Z. Yang and M. A. Sheremet. (2019). Numerical study of MHD nanofluid natural convection in a baffled U-shaped enclosure. International Journal of Heat and Mass Transfer, 130: 123-134.

Obalalu, A. M. (2021) Heat and mass transfer in an unsteady squeezed Casson fluid flow with novel thermophysical properties: Analytical and numerical solution. Heat Transfer, 50(8):7988-8011.

Olayemi, O.A.; M. Isiaka; K. Al-Farhany; M. A. Alomari; M. A. Ismael and S.O. Oyedepo. (2022a). Numerical Analysis of Natural Convection in a Concentric Trapezoidal Enclosure Filled with a Porous Medium. International Journal of Engineering Research in Africa, 61: 129-150.

Olayemi, O. A.; J. T. Olabemiwo; J. O. Dirisu; O. V. Ogunwoye; T. S. Jolayem; B. E. Anyaegbuna and T. A. Olaniyan. (2022b). Numerical simulation of heat transfer and fluid flow around a cylinder of varying cross-section. Materials Today: Proceedings, 65 (3):2128-2137.

Olayemi, O.A.; K. Al-Farhany; A.M. Obalalu; T. F. Ajide and K. R. Adebayo. (2022c). Magnetoconvection around an elliptic cylinder placed in a lid-driven square enclosure subjected to internal heat generation or absorption. Heat Transfer, 51:4950-4976.

Olayemi, O. A., A. Salaudeen; K. Al-Farhany; R. O. Medupin and I. K. Adegun. (2022d). Modelling of heat transfer characteristics around a cylindrical-barrier. International journal for engineering modelling, 35(1): 83-106.

Olayemi, O. A.; A. F. Khaled; O. J. Temitope; O. O. Victor; C. B. Odetunde and I. K. Adegun. (2021a). Parametric study of natural convection heat transfer from an inclined rectangular cylinder embedded in a square enclosure. Australian Journal of Mechanical Engineering, 1-14.

Olayemi, O. A.; J. T. Olabemiwo; T. S. Jolayemi; K. O. Oladosu; C. Odetunde and I. K. Adegun. (2021b). Computational fluid dynamics (cfd) analysis of buoyancy flow in a differentially heated square cavity. In IOP Conference Series: Material Science Engineering (Vol. 1107, No.1, p. 012120). IOP Publishing.

Olayemi, O. A., K. Al-Farhany; O. Olaogun; M. O. Ibiwoye; R. O. Medupin and A. Jinadu (2021c). Computational fluid dynamics analysis of mixed convection heat transfer and fluid flow in a lid-driven square cavity subjected to different heating conditions. In IOP Conference Series: Material Science Engineering (Vol. 1107, No. 1, p. 012201). IOP Publishing.

Pandey, S.; Y. G. Park and M. Y. Ha. (2020). Unsteady analysis of natural convection in a square enclosure filled with non-Newtonian fluid containing an internal cylinder. Numerical Heat Transfer, Part B: Fundamentals, 77(1):1-21. https://doi.org/10.1080/10407790.2019.1685838

Pratap Singh, M.; A. Rajvanshi and H. Thakur. (2020). Patterns of Natural Convection in an Irregular Arc-Shaped Enclosure. Heat Transfer Engineering, 41(6-7): 676-689. https://doi.org/10.1080/01457632.2018.1546987

Ragui, K.; Y. Benkahla; N. Labsi and A. Boutra. (2013). Natural heat transfer convection in a square cavity including a square heater. 21th Congrès Français de Mécanique, Bordeaux, 26.

Raizah, Z. A. S.; A. M. Aly and S. E. Ahmed. (2018). Natural convection flow of a power-law non-Newtonian nanofluid in inclined open shallow cavities filled with porous media. International Journal of Mechanical Sciences, 140:376-393. https://doi:10.1016/j.ijmecsci.2018.03.017.

Rehhali, K.; M. Hasnaoui; A. Raji; A. El-Mansouri; H. Beji; A. Amahmid and Y. Dahani. (2019). Lattice Boltzmann Approach for Natural Convection and Radiation in a Tilted Square Cavity. Journal of Thermophysics and Heat Transfer, 33(2): 322-333. https://doi.org/10.1080/01457632.2020.1723846.

Saeid, N. H. (2018). Natural convection in a square cavity with discrete heating at the bottom with different fin shapes. Heat Transfer Engineering, 39(2): 154-161. https://doi.org/10.1080/01457632.2017.1288053

Sheikholeslami, M.; T. Hayat and A. J. I. J. O. H. Alsaedi. (2017). On simulation of nanofluid radiation and natural convection in an enclosure with elliptical cylinders. International Journal of Heat and Mass Transfer, 115: 981-991.

Zhang, T., and Che, D. (2014). Lattice Boltzmann simulation of natural convection in an inclined square cavity with spatial temperature variation. Numerical Heat Transfer, 66(6): 712-732. https://doi.org/10.3329/jname.v15i1.33549